Available online at www.sciencedirect.com
SCIENCE DIRECT
Polymer 46 (2005) 3407–3418
polymer
www.elsevier.com/locate/polymer

Electrospinning of poly(MMA-*co*-MAA) copolymers and their layered silicate nanocomposites for improved thermal properties

M. Wang[a], A.J. Hsieh[b], G.C. Rutledge[a,*]

[a]*Dept. of Chemical Engineering, Massachusetts Institute of Technology, Cambridge, MA 02139, USA*
[b]*Army Research Laboratory, AMSRD-ARL-WM-MD, Aberdeen Proving Ground, MD 21005-5069, USA*

Received 2 December 2004; received in revised form 22 February 2005; accepted 28 February 2005
Available online 23 March 2005

Abstract

Copolymers consisting of methyl methacrylate (MMA) and methacrylic acid (MAA) and their layered silicate nanocomposites were electrospun to form fibers with diameters in the sub-micron range. The presence of MAA increased the T_g and thermal stability of the copolymers through formation of anhydrides upon heating. Fibers of uniform diameters were obtained for the poly(MMA-*co*-MAA) copolymers and nanocomposites containing montmorillonite (MMT), while protrusions were observed on the electrospun fibers from nanocomposites containing fluorohectorite (FH). The electrospinnability of copolymer solutions and nanocomposite dispersions predicted based on both rheological analyses and conductivity measurements correlates well with the experimental electrospinning observations. Dispersion of clays within the nanocomposites improved the electrospinnability of the nanocomposite dispersions. MMT is predominantly exfoliated and well distributed within the fiber and oriented along the fiber axis. Char formation was observed when the MMT-containing fibers were heated above the decomposition temperature, indicating a potential for reduced flammability and increased self-extinguishing properties, whereas the FH-containing materials disintegrated into either film or powder form.

Keywords: Electrospinning; Nanocomposite; Nanofiber

1. Introduction

Property enhancement of polymeric materials, including tailoring of thermal stability, mechanical strength and barrier properties, has been often pursued for engineering structural applications through such methods as copolymerization, melt-blending and incorporation of inorganic fillers. Poly(methyl methacrylate), PMMA, has excellent optical clarity, high mechanical strength and good weatherability, and is used widely as a transparent engineering material. However, the onset of thermal degradation of PMMA occurs at about 250–300 °C in air, and it decomposes completely to monomers when heated above this temperature [1]. The thermal stability of PMMA can be improved through copolymerization of methyl methacrylate (MMA) with methacrylic acid (MAA). Poly(methacrylic acid) (PMAA) has a higher glass transition temperature than PMMA [2], and it also exhibits a higher degradation temperature due to formation of anhydride upon heating [3]. The glass transition temperature and thermal stability of the resulting poly(MMA-*co*-MAA) copolymers can be tailored by adjusting the monomer contents. PMAA has been reported to be miscible with PMMA [2]; however, the degree of homogeneity was found to be much higher in the in situ polymerized random copolymers than in the corresponding physical blends. This was rationalized in terms of hydrogen bonding present between the carbonyl groups of MMA and MAA, and the extent of this intermolecular interaction was shown to be much higher in the copolymers than in the blends [2].

Incorporation of small levels of layered silicates (i.e. clays) into a polymer matrix has shown great promise for yielding nanocomposites with enhanced mechanical strength, chemical resistance, thermal stability, and self-extinguishing flammability characteristics compared to the pristine polymers [4–10]. These property improvements are attributed to the nanometric thickness and high aspect ratio of the individual clay platelets, as well as to the

* Corresponding author
E-mail address: rutledge@mit.edu (G.C. Rutledge).

0032-3861/$ - see front matter © 2005 Elsevier Ltd. All rights reserved.
doi:10.1016/j.polymer.2005.02.099

nanocomposite morphology with the platelets being exfoliated and well-dispersed. The high aspect ratio of clay platelets allows their nanocomposites to form a percolated mesoscale-structure at low volume fraction. However, it is more difficult to achieve complete exfoliation for layered silicates with high aspect ratio [10], which offsets some of the advantages of working with these materials. The common approaches undertaken to achieve exfoliated nanocomposite structures include modification of the clay surface chemistry from hydrophilic to organophilic in order to improve compatibility with the host polymer matrix, as well as utilization of special processing techniques, such as in situ polymerization, high shear solution blending or melt blending, to achieve delamination of the large stacks of silicate nanoparticles into isolated (i.e. exfoliated) platelets or 'tactoids' consisting of only a small number of platelets. In situ free-radical polymerization to incorporate montmorillonite (MMT) into the PMMA was first demonstrated by Blumstein [11]. Over the last several years, many other research groups have utilized this synthesis route to create PMMA nanocomposites with better exfoliation of layered silicates [9,12–15].

Electrospinning is an effective method for the production of polymeric fibers with diameters ranging from tens of nanometers to microns [16,17]. This technique has attracted great interest over the last decade due to the potential applications of nanofibers (i.e. fibers with diameters below 100 nm, and whose material properties exhibit a distinct size dependence) in such areas as molecular electronics [18–20], filtration [21,22], tissue engineering [23–26], sensors [27], protective clothing [28], and reinforcing components in nanocomposites [29–31]. The feasibility of incorporation of nanometer-sized particulates into fibers has made this process even more attractive for the production of composite fibers [32–36]. Orientation of the filler particles within the fibers during processing creates the possibility for manipulation of nanoparticles through appropriate handling of the fibers in which they are embedded and oriented. The critical material parameters for manufacturing such composite fibers include the type and geometry of the fillers, and the extent of homogeneous dispersion of filler within the polymer solution. Electrospinning of polymer layered-silicate nanocomposite into fibers was first demonstrated by Fong et al. [37]. They first compounded nylon-6 nanocomposites with MMT by melt processing, and then used hexafluoro-2-propanol (HFIP) or a mixture of HFIP and dimethylformamide (DMF) to prepare nanocomposite dispersions for electrospinning. The degree of dispersion and morphology of MMT in the resulting fibers were characterized, but no fiber properties were reported.

In electrospinning, a solidified fiber is formed from an electrically charged polymer liquid jet in the presence of an external electric field. The electrically charged liquid jet accelerated by the external electric field travels in a straight line, and then undergoes a whipping instability that leads to stretching of the jet before it hits a grounded collector [38–44]. 'Electrospinnability' of a polymer solution can thus be defined as the ability to form a continuous jet that is stable against breakup into droplets, in the presence of an electric field [43]. During the electrospinning process, a Rayleigh instability driven by the surface tension, which tends to break the jet into droplets, can develop along the thin liquid jet. This instability becomes more important as the diameter of the jet becomes smaller [38,39,43]. The external electric field accelerates the electrically charged jet and stretches it along the field axis, while the repulsive forces resulting from the surface charges lead to bending of the jet and stretching in the direction normal to the electric field. These two forces depend strongly on the total charge density of the jet, with most of the charge believed to reside at the jet surface. External electric field, surface charge and solution viscoelasticity tend to suppress the Rayleigh instability and stabilize the jet [38,39,43]. As a result, the surface tension, the charge density and the solution viscoelasticity are thought to play important roles in determining the electrospinnability of polymer solutions [44–46].

The objective of this work is to develop PMMA-based fibers with improved thermal properties by electrospinning. Specifically, we describe the formation by electrospinning of fibers from solutions of poly(MMA-*co*-MAA) copolymers and from dispersions of their layered-silicate nanocomposites. For comparison, fibers were also formed from solutions of homopolymer PMMA and homopolymer PMAA. The nanocomposites were prepared by in situ emulsion polymerization to enhance the dispersion and exfoliation of clay in the polymer matrix. The as-polymerized nanocomposites were then dispersed into solutions of dimethylformamide (DMF), from which fibers were electrospun. Two types of clays, pristine MMT and pristine fluorohectorite (FH) without any organic modifiers, were used to study the effect of lateral dimension of the clay platelets on fiber formation. The electrospinnability of the polymer solutions and nanocomposite dispersions can be understood in terms of their extensional rheology and conductivity properties. The morphology and thermal properties of the electrospun fibers are also reported.

2. Experimental

2.1. Materials preparation

The poly(MMA-*co*-MAA) copolymers containing nominally 100, 75, 50, 25 and 0 wt% MMA, and layered silicate nanocomposites with the same nominal compositions, were prepared individually via emulsion polymerization; the details of synthesis can be found elsewhere [47]. In brief, for the preparation of nanocomposites, 5 weight percent (wt%) of layered silicate per mass of monomer was premixed vigorously in water under nitrogen to promote exfoliation prior to the addition of monomers and initiator for polymerization. The layered silicates used include Na^+

montmorrilonite, MMT, (Southern Clay Products, Inc.) with cation exchange capacity (CEC) about 93 mequiv./100 gm clay and fluorohectorite, FH, (Corning, Inc.) with CEC about 180 mequiv./100 gm clay. MMT is a smectic aluminosilicate with average platelet diameter 0.1–1 μm, while FH is a synthetic, layered magnesium-silicate with a higher aspect ratio and an average platelet diameter about 4–5 μm [10]. The resulting neat polymer and silicate–polymer nanocomposites were then precipitated in methanol and dried to yield samples in the form of powder. Molecular weights of the neat PMMA and PMAA homopolymers were measured by gel permeation chromatography.

2.2. Electrospinning

Polymer solutions of 6 and 8% by weight were prepared by directly adding the neat polymers to dimethylformamide (DMF). The solutions were vigorously stirred for at least 24 h at room temperature. Nanocomposite dispersions were also prepared by dispersing the silicate–polymer nanocomposites at concentrations of 6 and 8 wt% in DMF. The dispersions were vigorously stirred for at least 72 h at room temperature. A parallel-plate electrospinning apparatus was used in this study, as described by Shin et al. [45] and Fridrikh et al. [48]. The electric field, solution flow rate and distance between the two parallel plates were adjusted to obtain a stable jet.

2.3. Fiber characterization

Images of fibers were taken using a JEOL-6060 scanning electron microscope (SEM) (JEOL Ltd, Japan). Transmission electron microscopy (TEM) of fibers was performed in a JEOL JEM200 CX TEM microscope (JEOL Ltd, Japan). Wide-angle X-ray diffraction (WAXD) data were obtained using a diffractometer (Bruker) with Cu K_α radiation at 40 kV and 20 mA. Small angle X-ray scattering (SAXS) data were obtained using a copper microfocused X-ray beam generator (Osmic Inc., MI) operated at 45 kV and 0.66 mA. The sample to detector distance was 1.3 m as calibrated using a silver behenate standard. Two-dimensional SAXS data were collected using a multi-wire detector (Molecular Metrology Inc., MA). Measurements of glass transition temperatures (T_g) were carried out using a Q1000 differential scanning calorimeter (TA Instrument Inc., DE) at a heating rate of 10 °C/min. T_g was determined based on the second heating scan preceded by a cooling scan at the same rate. Thermal stability of electrospun fibers was performed using a Perkin–Elmer thermogravimetric analyzer (TGA 7) at a heating rate of 20 °C/min. Dynamic light scattering (DLS) measurements were performed on a BI-9000AT spectrometer (Brookhaven Instrument Corp., NY). For DLS measurements, nanocomposite dispersions of 0.5 wt% in DMF were centrifuged using a Centrifuge 5804R (Eppendorf AG, Germany) at 5000 rpm for 15 min. The top portion of solution was taken out by a syringe and filtered using 0.1 μm Puradisk™ PTFE filter (Whatman plc, UK) for DLS measurements. The 5050-copolymer at 0.5 wt% in DMF was also used for DLS measurement.

2.4. Solution rheology

Shear rheology was performed on an AR2000 Rheometer (TA Instruments) at 25 °C using a parallel plate geometry with 40 mm diameter plates. Steady shear measurements were carried out at constant shear rates ranging from 1 to 1000 s^{-1}. Low amplitude oscillatory shear measurements were performed by applying a time dependent strain of $\gamma(t)=\gamma_0 \sin(\omega t)$, where ω is the frequency and t is the time. The resulting time dependent shear stress is $\tau(t) = \gamma_0[G' \sin(\omega t) + G'' \cos(\omega t)]$ where G' is the storage modulus, and G'' is the loss modulus. The linear viscoelastic moduli reported here were ensured to be independent of the strain amplitude by repeating measurements at two different strain amplitudes of 1 and 2%. Extensional rheological measurements were performed on a HAAKE CABER 1 rheometer (Thermo Electron Corporation, WI). In these measurements, the solution was first loaded into a gap of 3 mm between two cylindrical plates with diameter of 6 mm, and then a 'necked' liquid bridge configuration was generated by rapidly separating the two cylindrical plates to 9 mm at a constant strain rate of 0.3 m/s. The evolution of midpoint filament diameter, $D_{mid}(t)$ was then recorded as a function of time after cessation of motion of the plates. From this data, the Hencky strain, ε, and apparent extensional viscosity, $\bar{\eta}(\varepsilon)$ were calculated using Eqs. (1) and (2), respectively [49–51]:

$$\varepsilon = 2 \ln\left(\frac{D_0}{D_{mid}(t)}\right) \tag{1}$$

$$\bar{\eta}(\varepsilon) = \frac{\gamma}{dD_{mid}(t)/dt} \tag{2}$$

where D_0 is the initial diameter of the filament at its midpoint and γ is the surface tension of solution. The fluid elasticity was assumed to be dominated by the slowest relaxation process. The dependence of the filament diameter on time can then be described using a balance of the surface tension and elastic forces, as shown in Eq. (3) [49–51]:

$$D_{mid}(t) = D_0\left(\frac{GD_0}{\gamma}\right)^{\frac{1}{3}} e^{-\frac{t}{3\lambda_c}} \tag{3}$$

where G is the elastic modulus of the filament and λ_c is the longest relaxation time of the solution. The quantity GD_0/γ is called the elastocapillary number [49].

3. Results and discussion

3.1. Material characterization

3.1.1. X-ray diffraction analysis of nanocomposites

Wide-angle X-ray diffraction (WAXD) patterns obtained

for the poly(MMA-*co*-MAA) nanocomposites containing MMT are shown in Fig. 1(a). No peaks are discernible for these materials except for the PMAA–MMT nanocomposite. A diffraction peak at $2\theta = 5.74°$ is visible in this nanocomposite, corresponding to a *d*-spacing of 1.54 nm. In order to confirm the morphology of the other MMT-containing nanocomposites, small angle X-ray scattering (SAXS) and TEM measurements were carried out. The lack of notable SAXS peaks in Fig. 2 indicates that there is no long-range order of clay structures in the MMT-containing nanocomposites. TEM results further confirm that MMT clays are well dispersed in the as-polymerized MMT-nanocomposites, and that they are predominantly exfoliated, except for some tactoids with intercalated structure present in the PMAA–MMT nanocomposite. Figs. 3(a) and (b) are the representative TEM micrographs for PMMA–MMT and PMAA–MMT nanocomposites, respectively. The WAXD patterns obtained for the corresponding FH-containing nanocomposites are shown in Fig. 1(b). A diffraction peak at 2θ ranging from 7.45 to 8.50°, corresponding to a Bragg spacing of 1.04–1.19 nm, is present in all diffractograms. No peaks in SAXS are seen for these nanocomposites (not shown). These data suggest that FH clays are intercalated in the FH-

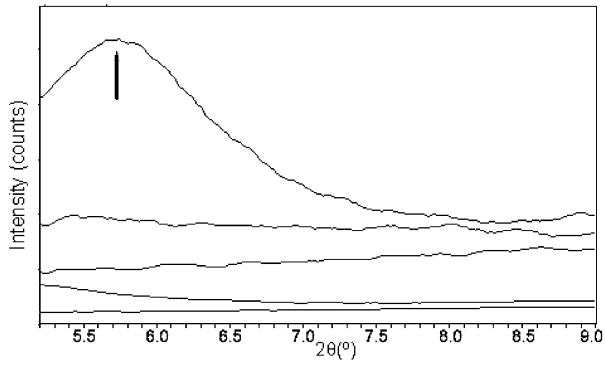

(a)

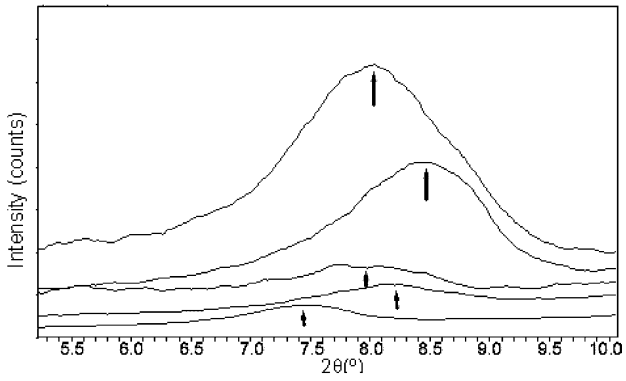

(b)

Fig. 1. Wide angle X-ray diffraction patterns of nanocomposites, the polymer matrix from bottom to top: PMMA, copolymers consisting of 75/25, 50/50, 25/75 weight ratio of MMA to MAA, and PMAA: (a) MMT-containing nanocomposites, (b) FH-containing nanocomposites. The peak positions are indicated by the arrows.

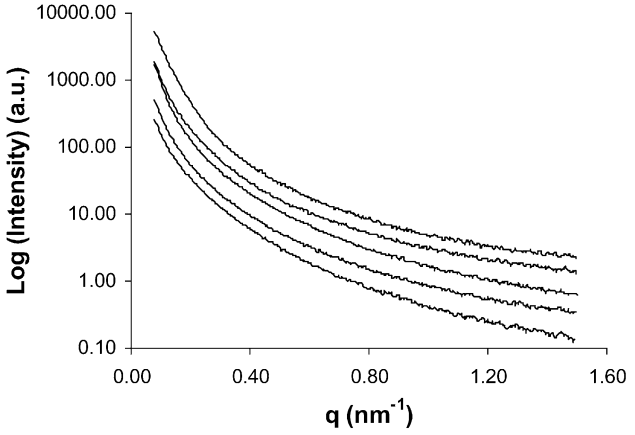

Fig. 2. SAXS data for the nanocomposites containing MMT, the polymer matrix from bottom to top: PMMA, copolymers consisting of 75/25, 50/50, 25/75 weight ratio of MMA to MAA, and PMAA.

containing nanocomposites as seen in Fig. 3(c) for the PMMA–FH nanocomposite, yet the tactoids are well dispersed. Thus, the as-polymerized MMT nanocomposites are better exfoliated than the corresponding FH-containing nanocomposites. MMT is a smectic clay consisting of layered aluminosilicate structures with lateral dimensions typically ranging from 0.1 to 1 μm, while FH is a synthetic, layered magnesium silicate with lateral dimensions around 4–5 μm, much larger than that of MMT [10]. These data suggest that the particle size might have played an important role affecting the ease of exfoliation of clay in the nanocomposites, even in the presence of in situ emulsion polymerization used here. For the purposes of electrospinning, the MMT and FH nanocomposites having a 50/50 weight ratio of MMA to MAA, denoted as 5050-copolymer nanocomposites, were selected in this work for the studies described below.

3.2. Rheology analysis

3.2.1. Shear rheology

The unfilled copolymers were completely dissolved in DMF, and transparent solutions were obtained. However, it was noticed that longer time was needed for PMAA to dissolve in DMF than for PMMA. Fig. 4 shows the results of steady shear viscosity vs. shear rate obtained for the PMMA, 5050-copolymer and PMAA solutions in DMF. The PMMA solution has the highest zero-shear-rate viscosity, followed by the 5050-copolymer, and PMAA the least. This is mainly due to a higher molecular weight of the PMMA synthesized ($M_w = 777{,}700$ g/mol) than that of PMAA ($M_w = 258{,}500$ g/mol).

When DMF was used as the solvent, a homogeneous translucent, gel-like dispersion was obtained for the 5050-MMT nanocomposite, while a white uniform dispersion was observed for the 5050-FH nanocomposite. Rheological measurements were carried out on these nanocomposite dispersions in DMF. Fig. 5 shows steady shear viscosity as a

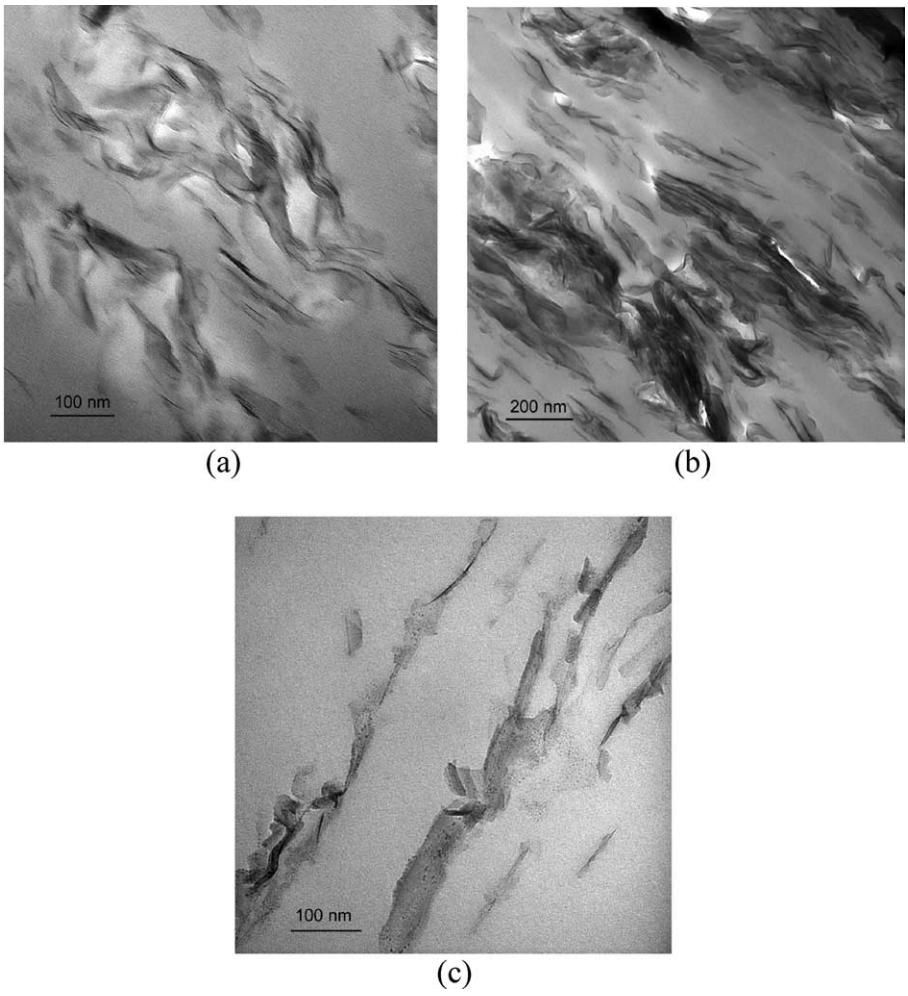

Fig. 3. Representative TEM images of nanocomposites (a) PMMA–MMT, (b) PMAA–MMT, (c) PMMA–FH.

function of shear rate. The 5050-MMT dispersion in DMF exhibits higher zero-shear-rate viscosity than the 5050-FH dispersion, yet both surpass the neat 5050-copolymer solution. We used dynamic light scattering to determine the hydrodynamic diameter of the neat 5050-copolymer and the 5050-copolymer matrix component extracted from the nanocomposites. The latter were obtained by dissolving the nanocomposites in DMF and subsequently removing the clay component through filtering. The results listed in Table 1 show that neat 5050-copolymer has the largest hydrodynamic diameter, followed by 5050-copolymer in

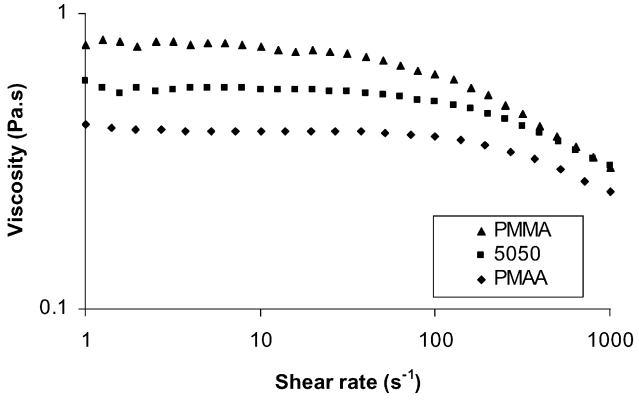

Fig. 4. Shear viscosity vs. shear rates of different polymer solutions.

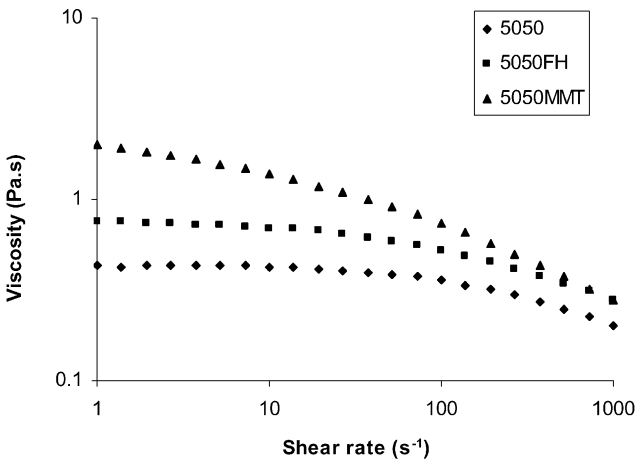

Fig. 5. Comparison of shear viscosity vs. shear rate of 5050-compolymer and their layered silicate nanocomposites.

the nanocomposite containing FH, and then by the nanocomposite containing MMT. Since the DLS measurements were conducted at the same polymer concentration in DMF, the order of hydrodynamic diameters reflects the order of molecular weights. Therefore, the higher shear viscosity observed in Fig. 5 for the nanocomposites dispersions is predominantly due to the incorporation of clay, and not the molecular weight of the copolymers. At low shear rates ($<50\ s^{-1}$, Fig. 5), pronounced non-Newtonian shear thinning, which is characteristic of layered silicate ordering in the flow direction [52,53], is observed in the 5050-MMT dispersion, but not in the 5050-FH dispersion. The latter exhibits predominantly Newtonian behavior, as does the 5050-copolymer solution. The extent of shear thinning at these low shear rates has been reported to correlate directly with the concentration of platelets and the extent of filler–filler interaction [52,54–56]. The particle size of FH is much larger than that of MMT; however, the effective anisotropy of the tactoids of FH may be compensated by the larger stack size or an intercalated silicate structure, indicated by WAXD, as compared to the tactoids of MMT. Based on this, our results from the steady shear rheological measurements suggest that MMT is more exfoliated than FH in the 5050-nanocomposite dispersions.

Fig. 6(a) and (b) shows that the values of storage modulus, G' and loss modulus, G'', obtained from the dynamic shear measurements for the 5050-MMT are substantially higher than those for the 5050-FH at all frequencies. The G' and G'' values for the latter in turn are slightly higher than those for the 5050-copolymer at all frequencies. Like shear viscosity, the dynamic moduli of nanocomposite dispersions depend not only on the properties of the polymer solution, but also on the interaction between clay particles and on the interaction between the clay and polymer solution [57–59]. The drastic increase in both moduli of the MMT nanocomposite can presumably be attributed to the better exfoliation of MMT compared to that of FH in the 5050-copolymer solutions [57]. This would be consistent with the results of steady shear rheology and WAXD analysis of as-polymerized nanocomposites.

3.2.2. Extensional rheology and conductivity measurements

The time evolution of the midpoint diameter of the fluid filament during the extensional deformation was investigated for the 8 wt% PMMA, 5050-copolymer and PMAA solutions, and for the 5050-copolymer nanocomposite dispersions in DMF (Fig. 7(a)). The capillary thinning of a fluid filament is a result of the competition of surface tension forces squeezing fluid from the filament and causing it to thin down, and polymer solution elasticity resisting extensional deformation [49–51,60]. A slower rate of capillary thinning is expected to correlate with better spinnability of the polymer solution. The data presented in Fig. 7(a) shows that the PMMA solution has a lower rate of capillary thinning than the 5050-copolymer and PMAA solutions. The values of apparent extensional viscosity vs. Hencky strain, calculated from the diameter vs. time data based on Eqs. (1) and (2), are shown in Fig. 7(b). Strain hardening is seen in all the polymer solutions upon extensional elongation. It is more pronounced in PMMA than in PMAA due to the high molecular weight of PMMA. In addition, results obtained from the conductivity measurements show that the PMMA solution has the highest conductivity compared to the 5050-copolymer and PMAA solutions in DMF. These observations would predict better electrospinnability for the PMMA solutions in DMF than for the 5050-copolymer and PMAA solutions, based on the expectation of a larger charge density from the conductivity measurement and a slower rate of capillary thinning from the extensional rheology analysis. Incorporation of clay apparently decreases the rate of capillary thinning of the nanocomposite dispersions as shown in Fig. 7(a), and strong

Table 1
Comparison of hydrodynamic diameters of the neat 5050-copolymer and the 5050-copolymers extracted from the 5050-MMT and 5050-FH nanocomposites

0.5 wt% in DMF	Hydrodynamic diameter (nm)
Neat 5050-copolymer	21.24±0.38
5050-Copolymer in FH nanocomposite	19.38±0.86
5050-Copolymer in MMT nanocomposites	13.7±1.74

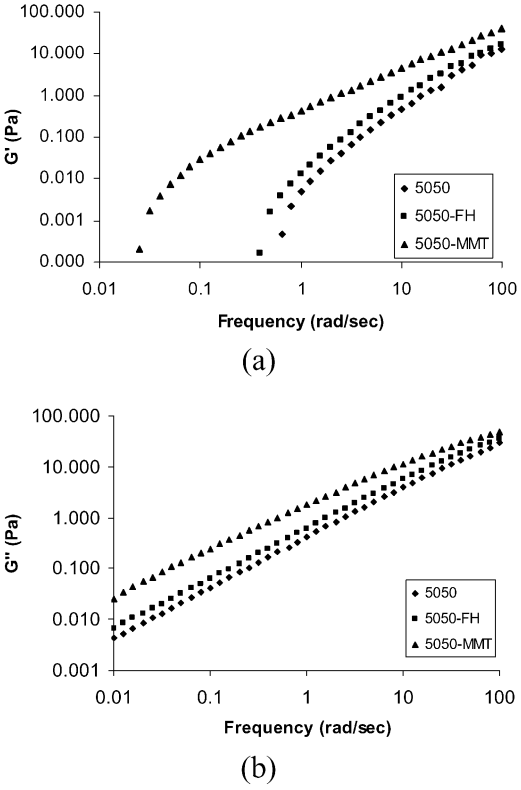

Fig. 6. (a) Storage modulus vs. frequency of 5050-copolymer and their layered silicate nanocomposites (b) loss modulus vs. frequency for the corresponding materials.

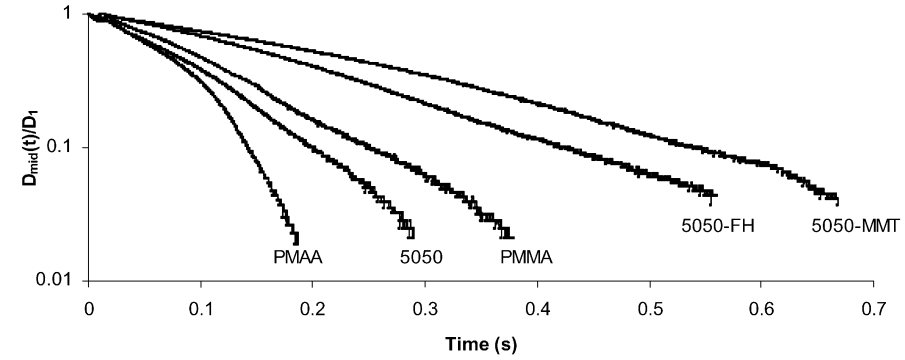

(a)

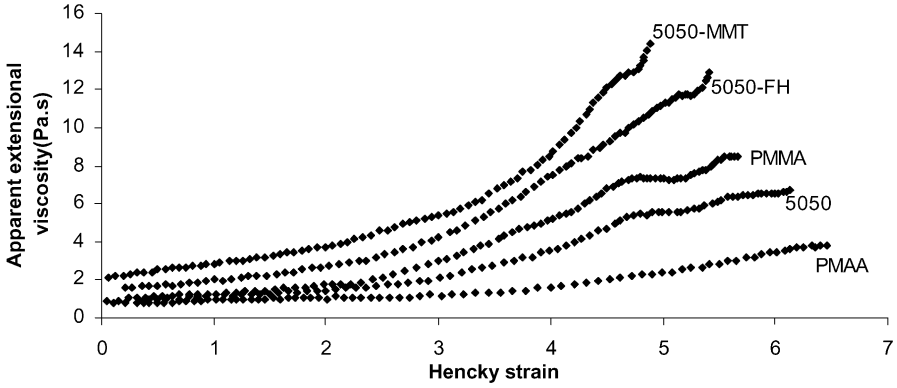

(b)

Fig. 7. (a) Evolution of midfilament diameter vs. time for the 5050-copolymers and their layered silicate nanocomposites (b) apparent extensional viscosity vs. Hencky strain for the corresponding materials.

strain hardening was observed for the 5050-MMT and 5050-FH dispersions (Fig. 7(b)). Meanwhile, incorporation of clay does not change significantly the conductivity of the nanocomposite dispersions (Table 2). As a result, the layered-silicate nanocomposite dispersions are expected to exhibit better electrospinnability than the corresponding polymer solutions.

An elastic model, described by Eq. (3), was used to fit the data from extensional rheology to determine the longest relaxation time, λ_c, associated with both polymer solutions and nanocomposite dispersions [49–51]. Table 3 lists the values of the relaxation times, λ_c, and the filament break up time t_b, obtained for these solutions and dispersions. Both the λ_c and t_b values associated with the nanocomposite dispersions are significantly higher than those of the unfilled polymers, presumably due to filler–filler and polymer–filler interactions [61,62]. In addition, the 5050-MMT dispersion exhibits a longer relaxation time and a longer experimental time to break than does the 5050-FH dispersion. We attribute this observation primarily to the difference in the extent of exfoliation of these clays, in accord with the results seen in the shear rheology analyses and WAXD patterns for as-polymerized nanocomposites.

3.3. Electrospinning

Typical processing parameters used to electrospin the neat polymer solutions and the 5050-copolymer nanocomposite dispersions at concentrations of 6 and 8% by weight are listed in Table 2. Fig. 8 shows representative SEM images of electrospun fibers. At 6 wt%, a beads-on-string morphology was obtained when the PMAA and 5050-copolymer solutions were spun (Fig. 8(a)), while a fiber morphology was achieved for the PMMA solution, 5050-MMT and 5050-FH dispersions. These results are consistent with the prediction of electrospinnablity of polymer solutions and nanocomposite dispersions based on the extensional rheology and conductivity measurements. For the 5050-MMT nanocomposite, uniform fibers were obtained, but nonuniformities were visible on some of the electrospun 5050-FH fibers (Fig. 8(d)). The latter is attributed to the dimension of the FH clays (about 4–5 μm) being significantly larger than the fiber diameter, resulting in large protrusions. Results of the TEM analysis indicate that the majority of intercalated FH structures are present in these nonuniformities rather than in the uniform sections of the fibers. At 8 wt% solutions, uniform fiber morphology was observed for the PMAA, 5050-copolymer

Table 2
Typical processing parameters used for electrospinning

	Conductivity (μs/cm)	Voltage (kV)	Distance (cm)	Flow rate (ml/min)	Current (nA)	Fiber diameter (nm)
PMAA (6 wt%)	24.6	19	25	0.03	80.3	Beads-on-string
5050-Copolymer (6 wt%)	68.0	19	30	0.015	64.2	Beads-on-string
PMMA (6 wt%)	94.0	17	30	0.015	103	550±60
5050-FH (6 wt%)	61.2	13	30	0.03	81.8	320±70 with protrusions
5050-MMT (6 wt%)	57.0	20	30	0.02	73.2	350±90
PMAA (8 wt%)	40.9	20	25	0.025	114.3	220±40
5050-Copolymer (8 wt%)	79.6	15.0	30	0.02	88.2	430±40
PMMA (8 wt%)	112.0	11.8	30	0.03	123	1400±120
5050-FH (8 wt%)	72.1	10.2	30	0.05	118.7	660±80 with protrusions
5050-MMT (8 wt%)	82.7	17.0	30	0.05	240.8	630±160

Conductivity refers to the static conductivity of solution; voltage refers to the applied voltage; distance refers to the separation between nozzle and collection electrodes; current refers to that measured at the collector electrode [44].

and PMMA solutions, and for the 5050-MMT dispersion; however, protrusions were still observed on some of the electrospun fibers from the 5050-FH nanocomposite dispersions (Fig. 8(h)).

3.4. Characterization of fibers

3.4.1. Morphology analysis

The morphology and the degree of dispersion of nanoclays within the fibers were characterized by TEM and wide-angle X-ray diffraction (WAXD). TEM results reveal that the majority of MMT platelets are exfoliated, and they are well distributed within the fiber volume and oriented along the fiber axis, as shown in Fig. 9(a). This clearly indicates the feasibility of electrospinning of the 2-D platelet structures and the potential to achieve proper alignment of these nanoclays along the fiber axis, which is critical for nanocomposite fiber fabrication [37]. Fewer FH clay particles are observed within the as-spun fibers, and most of these appear to be in tactoids and to reside near the edge of the fibers, as shown in Fig. 9(b). They are nevertheless well aligned in the fiber direction.

Wide-angle X-ray diffraction patterns of fibers were obtained using the electrospun non-woven mats. Fig. 10 shows that a small peak is barely observable at $2\theta = 6.68°$, with a corresponding d-spacing value of 1.31 nm, for the 5050-MMT, and at $2\theta = 7.62°$, with d-spacing of 1.16 nm, for the 5050-FH. The position of the basal reflection associated with the FH is about the same for both the as-polymerized 5050-FH nanocomposite and the as-spun 5050-FH fibers. On the other hand, a small peak appears for the as-spun fibers of 5050-MMT that was not seen in the as-polymerized 5050-MMT nanocomposite. A similar WAXD pattern with a basal reflection at $2\theta = 6.40°$ was also noticed for a solution cast film of 5050-MMT in DMF (not shown). Therefore, the change of MMT morphology between the as-polymerized nanocomposites and electrospun fiber is probably due to the effect of DMF solvent on the extent of exfoliation of clay in the nanocomposite dispersions. The latter was also noted by Fong et al. when they prepared nylon-MMT nanocomposite dispersions in a mixture of HFIP and DMF solvents [37]. They suggested that solvents presumably cause desorption of polymer molecules from the silicate surface and lead to the aggregation of layered silicates.

Table 3
Comparison of the longest relaxation time and time to break for different solutions or dispersions

8 wt% in DMF	λ_c (s)	t_b (s)
PMAA	1.18×10^{-2}	0.312
5050-Copolymer	2.73×10^{-2}	0.337
PMMA	3.57×10^{-2}	0.442
5050-FH	5.38×10^{-2}	0.677
5050-MMT	6.96×10^{-2}	0.824

3.4.2. Thermal analysis of fibers

Fig. 11 displays the DSC thermographs obtained for electrospun fibers of PMMA and PMAA homopolymers, 5050-copolymer, 5050-MMT and 5050-FH nanocomposites. The glass transition temperatures, T_g's, of these materials determined from the second heating scan are compared in Table 4. A single T_g is observed for all the fibers electrospun from 5050-copolymer and their nanocomposites indicating miscibility between MMA and MAA molecules at least on the scale of thermal conduction length 20–30 nm. These fibers comprising 5050-copolymer based materials exhibit an increase in T_g of about 26–28 °C over that of the PMMA fiber. These results are consistent with the DSC results obtained for the as-polymerized poly(MMA-*co*-MAA) copolymers [47]. It is noteworthy that T_g's of 5050-copolymer containing fibers are much closer to the T_g of PMAA fiber than that of PMMA fiber. PMAA aforementioned undergoes anhydride formation upon heating [3]. This reaction presumably occurred during the first heating scan of PMAA-containing materials in DSC. As a result, T_g of these materials can only be determined from the following heating scan after the completion of anhydride formation. Therefore, the T_g values determined from the second

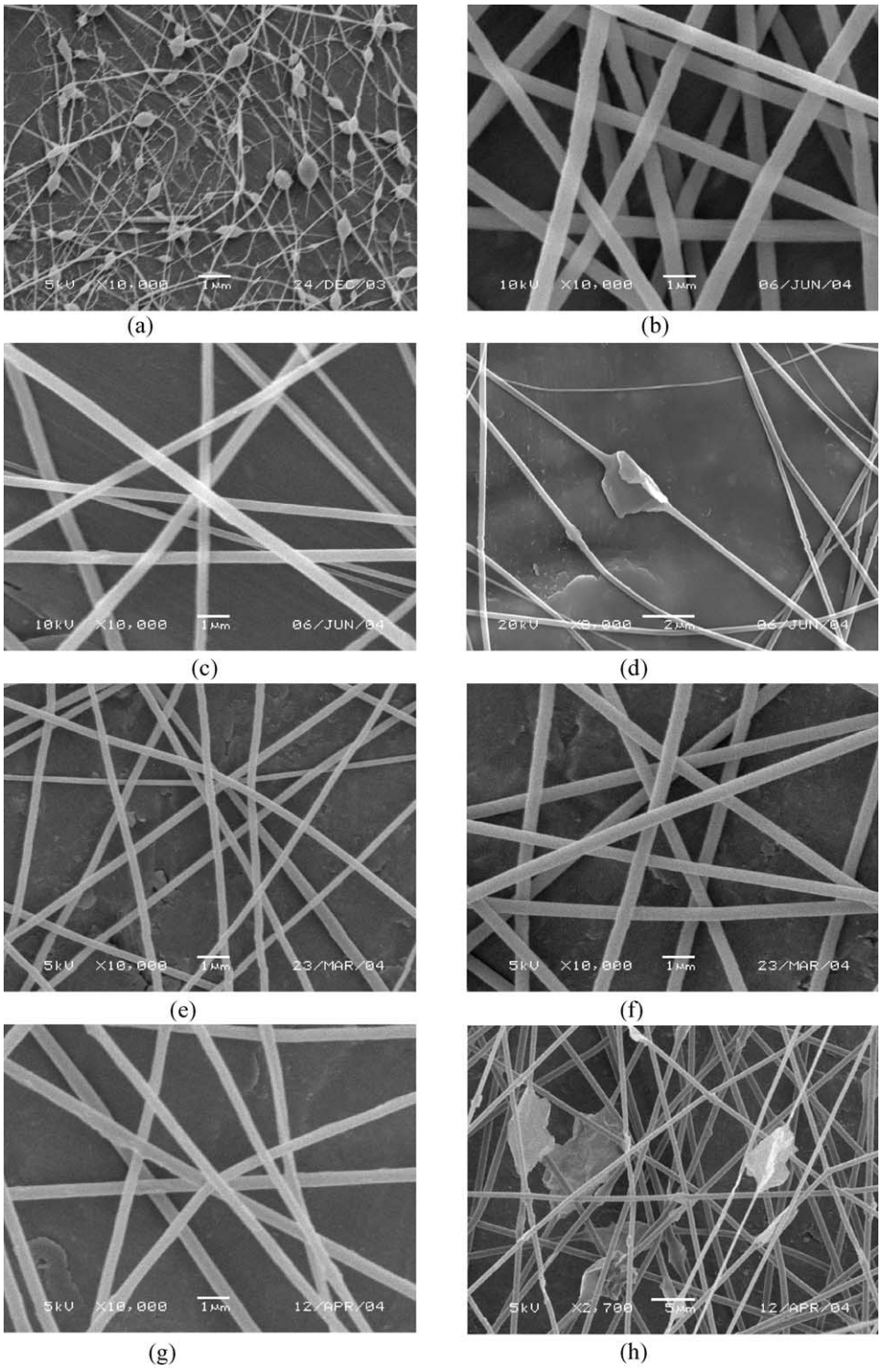

Fig. 8. Representative SEM images of electrospun fibers from the following solutions in DMF: (a) 5050-copolymer (6 wt%), (b) PMMA (6%), (c) 5050-MMT (6%), (d) 5050-FH (6%), (e) PMAA (8%), (f) 5050-copolymer (8%), (g) 5050-MMT (8%), (h) 5050-FH(8%).

heating scan in DSC reflect the thermal characteristics of materials presumably in the form of anhydrides of PMAA homopolymer or 5050-copolymer, which haven't been reported in the literature to date.

Thermal stability of the electrospun fibers was evaluated using TGA in nitrogen atmosphere. For comparison, a thermally pressed homopolymer PMMA film was also tested by TGA under the same conditions. The TGA data of weight change and the derivative of weight change for the homopolymer PMMA film are shown in Fig. 12. Two steps

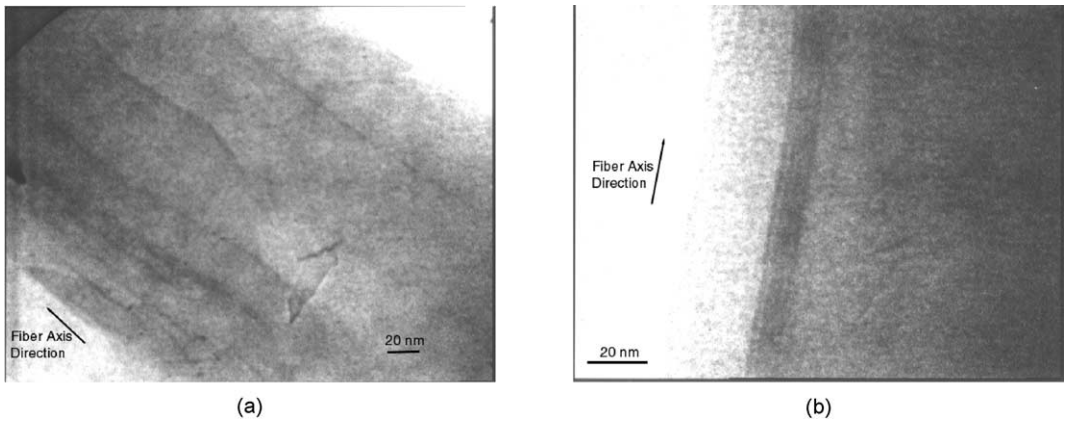

Fig. 9. Representative TEM images of electrospun fibers from the following solutions in DMF: (a) 5050-MMT (6%), (b) 5050-FH (6%).

of degradation process are observed, indicated by two peaks in the derivative of weight change plot. The first thermal degradation of PMMA film in nitrogen, indicated by a small peak in the range 270–390 °C, is presumably due to the thermal degradation of less stable head-to-head linkages and unsaturated vinyl end groups in the PMMA molecular chains, as reported for PMMA synthesized by free-radical polymerization [1]. The second thermal degradation, indicated by a large peak at about 470 °C, is due to the complete decomposition of polymer main chains. The weight change as a function of temperature for different electrospun fibers are compared in Fig. 13. The degradation curve for PMMA fiber shows a similar two-step degradation process as seen for the melt-processed PMMA film, except that the former exhibits slightly better thermal stability indicated by a lesser extent of weight loss associated with the first step degradation in the temperature range of 270–390 °C. This minor difference may be partly due to the variation in processing (melt-compression vs. solvent-assisted electrospinning), the details of which remain the subject for further investigation. The fibers containing 5050-copolymer reveal the onset of weight loss at much lower temperature than the PMMA fiber. The small weight loss between room temperature and about 100 °C is a result of the release of adsorbed water due to the hydrophilic nature of MAA components. The weight loss between about 100 and 270 °C is due to the release of water and CH_3OH molecules from anhydride formation between MAA units and between the carboxyl group of MAA and the carboxylate group of MMA in the poly(MMA-*co*-MAA) copolymers, respectively [3]. The extent of the MAA–MMA anhydride formation presumably depends upon the proximity of reactive monomers resulting from copolymerization, the tacticity of these monomer units, and the polymer chain conformation. The weight loss between 270 °C and the onset temperature of thermal degradation of polymer main chains, indicated by the significant weight loss in TGA, is the result of possibly continual anhydride formation between MAA and MMA molecules as well as the degradation of the weak linkages of MMA components as discussed above. The anhydrides formed during TGA subsequently result in an increase in the thermal stability of 5050-copolymer based fibers. These materials exhibit an onset of thermal degradation of polymer main chains almost 80 °C higher than that of the PMMA fiber. The 5050-MMT fibers charred after being heated to 800 °C in nitrogen while

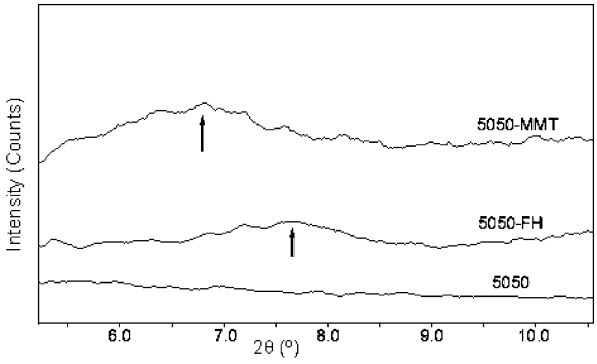

Fig. 10. Comparison of WAXD patterns of 5050-copolymer, 5050-FH and 5050-MMT electrospun fibers. The peak positions are indicated by the arrows.

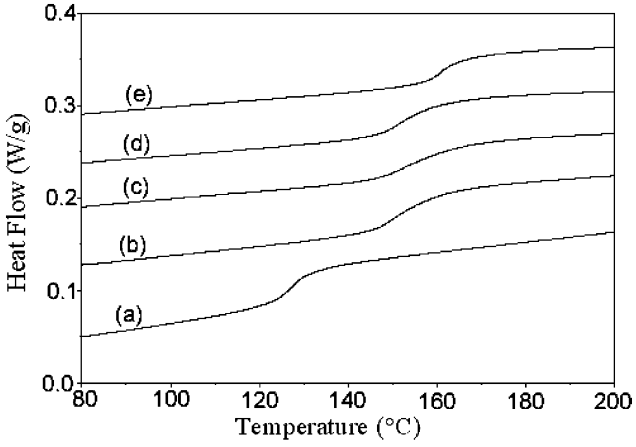

Fig. 11. DSC thermograms obtained from the second heating scan for electrospun fibers (a) PMMA, (b) 5050-copolymer, (c) 5050-FH nanocomposite, (d) 5050-MMT nanocomposite, (e) PMAA.

Table 4
T_g of electrospun fibers

Electrospun fiber	T_g (°C)
PMMA	127.1
5050-Copolymer	152.9
5050-FH	155.4
5050-MMT	153.5
PMAA	161.7

a film formation was noted in the 5050-FH fibers (Fig. 14); the remaining wt% of char residues as shown in Fig. 12 is about 4.8% and 4.2% for the 5050-MMT and 5050-FH fibers, respectively. Gilman et al. [10] also noted a difference in the char formation behavior during burning of MMT and FH based nanocomposites. They attributed this to the smaller size of the MMT lamellae, which could presumably facilitate the reassembly of lamellae to form three-dimensional char. The MMT char could act as an excellent insulator and mass transport barrier and subsequently mitigate the escape of volatile products generated during polymer decomposition. This char is desired to reduce the flammability and increase the self-extinguishing property of nanocomposite fibers [10].

4. Conclusions

Fibers of poly(MMA-*co*-MAA) copolymers and their layered silicate nanocomposites were prepared by electrospinning. The copolymers containing MAA exhibit enhanced T_g and thermal stability through formation of anhydrides upon heating. The clays in the nanocomposite dispersions increase the zero-shear-rate viscosity over that of the pristine polymers. Both steady and transient shear rheology data reveal that MMT is more exfoliated than FH in the 5050-nanocomposite dispersions, which is attributed to the difference in the lateral size of the clays. The electrospinnability of copolymer solutions and nanocomposite dispersions predicted based on data from both extensional viscometry and conductivity measurements correlates well with the production of uniform fibers. Dispersion of clays within the nanocomposites improved the electrospinnability of these materials through increased apparent extensional viscosity and strain hardening. Uniform fibers with diameters in the sub-micron range were obtained for the 5050-copolymer and 5050-MMT nanocomposite, while existence of protrusions is observed in electrospun 5050-FH fibers, due to the large size of the FH clay platelets. MMT is predominantly exfoliated and well distributed within the fiber volume and along the fiber axis; however, fewer FH platelets are observed within the fiber and most of them appear to be intercalated. In addition, the fibers containing well-dispersed and predominantly exfoliated MMT clays char upon decomposition. Thus, through electrospinning of dispersions of copolymers of MMA and MAA synthesized in situ with clays, a novel fiber with high glass transition temperature and enhanced thermal stability has been demonstrated, with potential to reduced flammability and improved self-extinguishing properties.

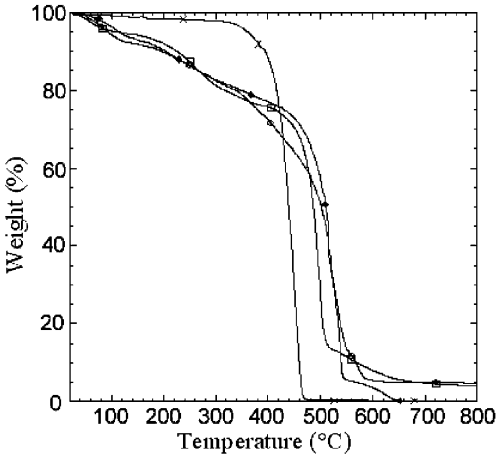

Fig. 13. Comparison of weight changes of electrospun fibers as a function of temperature for PMMA (×), 5050-copolymer (♦), 5050-MMT (○), 5050-FH (□) nanocomposites.

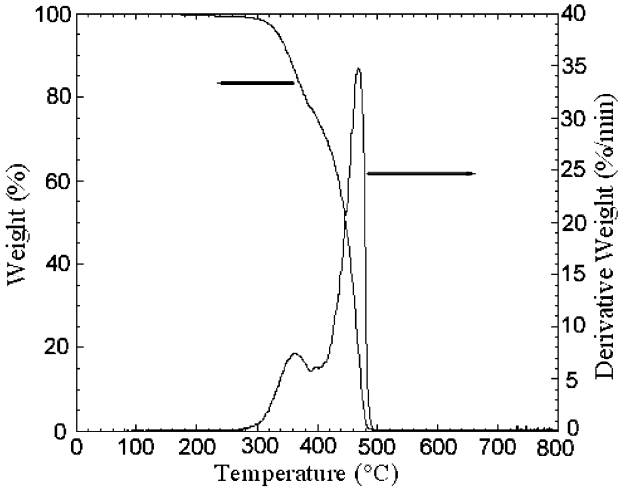

Fig. 12. Weight change (%) and derivative of weight change (%/min) as a function of temperature for melt processed PMMA film.

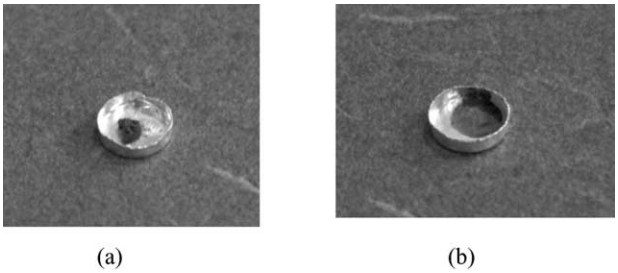

Fig. 14. Comparison of TGA residues of electrospun fibers: (a) 5050-MMT, (b) 5050-FH.

Acknowledgements

The poly(MMA-*co*-MAA) nanocomposites were kindly made available by E. Giannelis at Cornell University through an earlier collaboration with AJH. Useful discussions with S.V. Fridrikh and J.H. Yu on extensional rheology and electrospinnability are gratefully acknowledged. This research was supported by the US Army through the Institute for Soldier Nanotechnologies, under Contract DAAD-19-02-D0002 with the US Army Research Office.

References

[1] Hirata T, Kashiwagi T, Brown JE. Macromolecules 1985;18:1410–8.
[2] Huang CF, Chang FC. Polymer 2003;44:2965–74.
[3] Ho BC, Lee YD, Chin WK. J Polym Sci, Polym Chem 1992;30: 2389–97.
[4] Usuki A, Kojima Y, Kawasumi M, Okada A, Fukushima Y, Kurauchi T, et al. J Mater Res 1993;8:1179–84.
[5] Kojima Y, Usuki A, Kawasumi M, Okada A, Fukushima Y, Kurauchi T, et al. J Mater Res 1993;8:1185–9.
[6] Messersmith P, Giannelis EP. Chem Mater 1993;5:1064–6.
[7] Giannelis EP. Adv Mater 1996;8:29–35.
[8] LeBaron PC, Wang Z, Pinnavaia TJ. Appl Clay Sci 1999;15:11–29.
[9] Deitsche F, Thomann R, Thomann R, Mulhaupt R. J Apply Polym Sci 2000;75:396–405.
[10] Gilman JW, Jackson CL, Morgan AB, Harris R, Manias E, Giannelis EP, et al. Chem Mater 2000;12:1866.
[11] Bumstein A. J Polym Sci 1965;A3:2665–72.
[12] Huang X, Brittain WJ. Macromolecules 2001;34:3255–60.
[13] Bandyopadhyay S, Hsieh AJ, Giannelis EP. ACS Symp Series 2002; 804:15–25.
[14] Okamoto M, Morita S, Taguchi H, Kim YH, Kotaka T, Tateyama H. Polymer 2000;41:3887–990.
[15] Fan XW, Xia CJ, Advincula RC. Langmuir 2003;19:4381–9.
[16] Doshi J, Reneker DH. J Electrostat 1995;35:151–60.
[17] Formhals A, US Patent No. 1,975,504.
[18] Norris ID, Shaker MM, Ko FK, MacDiarmid AG. Synth Met 2000; 114:109–14.
[19] MacDiarmid AG, Jones Jr WE, Norris ID, Gao J, Johnson Jr AT, Pinto NJ, et al. Synth Met 2001;119:27–30.
[20] Reneker DH, Chun I. Nanotechnology 1996;7:216–23.
[21] Tsai PP, Schreuder-Gibson H, Gibson P. J Electrostat 2002;54: 333–41.
[22] Demir MM, Yilgor I, Yilgor E, Erman B. Polymer 2002;43:3303–9.
[23] Jin HJ, Fridrikh SV, Rutledge GC, Kaplan DL. Biomacromolecules 2002;3:1233–9.
[24] Huang L, McMillan RA, Apkarian RP, Pourdeyhimi B, Conticello VP, Chaikof EL. Macromolecules 2000;33:2989–97.
[25] Matthews JA, Wnek GE, Simpson DG, Bowlin GL. Biomacromolecules 2002;3:232–8.
[26] Boland ED, Wnek GE, Simpson DG, Pawlowski KJ, Bowlin GL. J Macromol Sci-Pure Appl Chem 2001;38(12):1231–43.
[27] Wang XY, Drew C, Lee SH. J Macromol Sci-Pure Appl Chem 2002; A39:1251–8.
[28] Gibson PW, Schreuder-Gibson HL, Rivin D. AIChE J 1999;45:190–5.
[29] Bergshoef MM, Vancso GJ. Adv Mater 1999;11:1362–5.
[30] Kim JS, Reneker DH. Polym Compos 1999;20:124–31.
[31] Zarkoob S, Eby RK, Reneker DH, Hudson SD, Ertley D, Adams WW. Polymer 2004;45:3973–7.
[32] Sen R, Zhao B, Perea D, Itkis ME, Hu M, Love J, Bekyarova E, Haddon RC. Nano Letters 2004;4:459–64.
[33] Ko F, Gogotsi Y, Ali A, Naguib N, Ye H, Yang G, et al. Adv Mater 2003;15:1161–5.
[34] Wang M, Singh H, Hatton A, Rutledge GC. Polymer 2004;45: 5505–14.
[35] Shao C, Kim HY, Gong J, Ding B, Lee DR, Park SJ. Mater Lett 2003; 57:1579–84.
[36] Yang QB, Li DM, Hong YL, Wang C, Qiu SL, Wei Y. Synth Met 2003;137:973–4.
[37] Fong H, Liu W, Wang CS, Vaia RA. Polymer 2002;43:775–80.
[38] Hohman MM, Shin M, Rutledge G, Brenner MP. Phys Fluids 2001; 13:2201–20.
[39] Hohman MM, Shin M, Rutledge G, Brenner MP. Phys Fluids 2001; 13:2221–36.
[40] Reneker DH, Yarin AL, Fong H, Koombhongse S. J Appl Phys 2000; 87:4531–47.
[41] Feng JJ. Phys Fluids 2002;14:3912–26.
[42] Yarin L, Koombhongse S, Reneker DH. J Appl Phys 2001;90: 4836–46.
[43] Yu JH, Fridrikh SV, Rutledge GC. Adv Mater 2004;16(17):1562–6.
[44] Shin YM, Hohman MM, Brenner MP, Rutledge GC. Polymer 2001; 42:9955.
[45] Shin M, Hohman MM, Brenner MP, Rutledge GC. Appl Phys Lett 2001;78:1149–51.
[46] Fong H, Chun I, Reneker DH. Polymer 1999;40:4585–92.
[47] Wang M, Hsieh AJ, Rutledge GC. Polym Mater Sci Eng 2004;91: 818–9.
[48] Fridrikh SV, Yu JH, Brenner MP, Rutledge GC. Phys Rev Lett 2003; 90:144502.
[49] Anna SL, McKinley GH. J Rheol 2001;45(1):115–38.
[50] McKinley GH, Brauner O, Yao M. Proc First Int Symp Appl Rheol, Korea 2001;18–19.
[51] Kolte M, Szabo P. J Rheol 1999;43:609–26.
[52] Krishnamoorti R, Ren J, Silva AS. J Chem Phys 2001;114:4968–73.
[53] Hyun YH, Lim ST, Choi HJ, Jhon MS. Macromolecules 2001;34: 8084–93.
[54] Wagener R, Reisinger TJG. Polymer 2003;44:7513–8.
[55] Solomon MJ, Almusallam AS, Seefeldt KF, Somwangthanaroj A, Varadan P. Macromolecules 2001;34:1864–72.
[56] Galgali G, Ramesh C, Lele A. Macromoecules 2001;34:852–8.
[57] Lim YT, Park OO. Rheol Acta 2001;40:220–9.
[58] Krishnamoorti R, Giannelis EP. Macromolecules 1997;30:4097–102.
[59] Ren IJX, Silva AS, Krishnamoorti R. Macromolecules 2000;33: 3739–46.
[60] Spiegelberg S, Ables D, McKinley G. J Non-Newtonian Fluid Mech 1996;64:229–67.
[61] Tanoue S, Utracki L, Garcia-Rejon A, Sammut P, Ton-That M, Pesneau I, et al. Polym Eng Sci 2004;44:1061–76.
[62] Prasad R, Pasanovic-Zujo V, Gupta R, Cser F, Bhattacharya S. Polym Eng Sci 2004;44:1220–30.